Research Article
https://doi.org/10.1631/jzus.B2400611

Regenerative potential of Schneiderian membrane-derived mesenchymal stem cells in sinus floor elevation model and calvarial defect model

Yuxin ZHAO[1*], Jia WANG[1*], Dongqi YOU[1], Yifan LU[1], Mengfei YU[1✉] and Misi SI[1✉]

[1]*Stomatology Hospital, School of Stomatology, Zhejiang University School of Medicine, Zhejiang Provincial Clinical Research Center for Oral Diseases, Key Laboratory of Oral Biomedical Research of Zhejiang Province, Cancer Center of Zhejiang University, Engineering Research Center of Oral Biomaterials and Devices of Zhejiang Province, Hangzhou 310000, China*

Abstract: Objectives: Schneiderian membrane-derived mesenchymal stem cells (SMMSCs) have been reported to be osteogenic progenitor cells in vitro. However, there is controversy regarding the intrinsic osteogenic capacity of the Schneiderian membrane, and the bone formation potential of SMMSCs in vivo has never been reported. Therefore, in this study we aimed to evaluate the contribution of the Schneiderian membrane to sinus floor elevation and to verify the function of SMMSCs in cranial bone defects. Materials and methods: Bilateral sinus floor elevation with chloromethyl-benzamidodialkylcarbocyanine (CM-DiI) labeling was performed in rabbits to assess Schneiderian membrane osteogenesis. Single-cell RNA sequencing was used to characterize human Schneiderian membrane cellular subsets. SMMSCs and bone marrow-derived mesenchymal stem cells (BMSCs) were transplanted into rabbit cranial defects with Gelatin Methacryloy (GelMA) scaffolds and analyzed via micro-CT and histology. Results: Spontaneous bone formation adjacent to the Schneiderian membrane was observed. Single-cell analysis identified paired related homeobox1 (*PRRX1*) progenitor clusters driving endo-sinus osteogenesis. SMMSCs exhibited superior earlier bone regeneration (4 weeks) compared with BMSCs, with higher tissue volume and bone volume/total volume (BV/TV) ratios. Conclusions: The Schneiderian membrane likely contributes to osteogenesis via *PRRX1*$^+$ progenitor lineages. SMMSCs promote accelerated early bone regeneration in cranial defects. This study provides the first in vivo validation of the osteogenic capacity of SMMSCs and defines their molecular identity at single-cell resolution.

Key words: Schneiderian membrane-derived mesenchymal stem cells; Single-cell RNA sequencing; Osteogenesis; Maxillary sinus floor elevation; Calvarial defect

1 Introduction

Owing to the insufficient bone height and poor bone quality in the maxillary posterior region, the placement of dental implants is often challenging, maxillary sinus floor elevation procedure has been widely performed by clinicians to solve this problem(Tatum, 1986; Summers, 1994; Al-Dajani, 2016; Hameed et al., 2019). The Schneiderian membrane, which covers the inner part of the maxillary sinus cavity, is elevated to create space for guiding bone regeneration(Pjetursson & Lang, 2014). While spontaneous bone formation following sinus elevation has attracted considerable research attention, the precise role of the Schneiderian membrane in endo-sinus bone augmentation remains controversial(Dragonas et al., 2020).

✉ Misi SI, misi_si@zju.edu.cn
Mengfei YU, yumengfei@zju.edu.cn
* Authors contributing equally to this article.
Misi SI, https://orcid.org/0000-0001-5352-2046
Mengfei YU, https://orcid.org/0000-0002-7700-4697

Received Dec. 2, 2024; Revision accepted Mar. 19, 2025
Crosschecked xxx. xx, 20xx; Published online xxx. xx, 20xx

Conflicting evidence exists regarding the osteoinductive potential of this membrane. Several studies concluded that the endo-sinus new bone tissue presented near the elevated Schneiderian membrane, indicating that with osteoinductive potential, the Schneiderian membrane may contribute to bone augmentation.(Palma et al., 2006; Moon et al., 2014; Rong et al., 2015). Conversely, Scala et al. reported that the Schneiderian membrane did not participate in new bone formation during healing events(Scala et al., 2010). The rabbit model has been extensively used to describe imitating bone healing processes after maxillary sinus floor elevation, owing to the species' anatomically favorable maxillary sinus characteristics that permit adequate space for bone formation(Asai et al., 2002; Yin et al., 2019; Leocadio et al., 2021; Lee et al., 2022). Therefore, we used a rabbit maxillary sinus floor elevation model to further explore the contribution of the Schneiderian membrane in bone augmentation.

The mechanisms underlying bone regeneration following sinus elevation remain incompletely understood. Emerging evidence the Schneiderian membrane-derived mesenchymal stem cells(SMMSCs) own the ability for osteogenic, adipogenic, and chondrogenic differentiation(Wang et al., 2022). These cells exhibited characteristic mesenchymal markers (*STRO-1*, *CD146*, *CD29*, *CD44*) and demonstrated functional similarities to other mesenchymal stem cells (MSCs) populations(Srouji et al., 2009; Guo et al., 2015). Recent investigations have identified $CD171^{+}/CD90^{+}$MSCs derived from lamina propria had stronger proliferative capacity, while $CD171^{-}/CD90^{+}$MSCs in the periosteal layer showed better osteogenic ability(Lv et al., 2024). Notably, Weng et al. identified the $Krt14^{+}Ctsk^{+}$ subset of cells in the Schneiderian membrane robustly contributed to maxillofacial bone regeneration in murine, which displayed both epithelial and mesenchymal properties.(Weng et al., 2022). The above studies demonstrated that the epithelial layer, lamina propria, and periosteal layer may have certain osteogenic potential. SMMSCs with specific molecular markers may be an important source of endogenic bone gain in the maxillary sinus. Thus, it is desirable to further characterize SMMSCs involved in the maxillary sinus new bone formation.

Isolated from various tissues and organs, MSCs are excellent candidates for cell therapy in tissue regeneration (Granchi et al., 2010; Lemos et al., 2015; Fujii et al., 2023). Bone marrow-derived mesenchymal stem cells (BMSCs) have been reported as practical seed cells for bone regeneration (Granchi, et al., 2010; Xie et al., 2022; Lee et al., 2023). However, allogeneic SMMSCs transplantation has not been reported. Whether SMMSCs could be suitable candidates for stem cell-based tissue engineering has not been examined. Therefore, we employed a well-established rabbit calvarial defect model to evaluate the bone regenerative capacity of scaffold-seeded SMMSCs(Saha et al., 2019; Liu et al., 2020) .

In this study, we aimed to provide further evidence for the osteogenic capacity of the Schneiderian membrane and to characterize specific MSCs subpopulations involved in sinus osteogenesis. We also aimed to assess the in vivo bone regenerative potential of allogeneic SMMSCs through calvarial defect repair and to provide new biological information on allogeneic SMMSCs transplantation. To our knowledge, this represents the first comparative investigation of SMMSCs versus BMSCs in bone regeneration models. We hypothesize that the Schneiderian membrane contains clinically relevant MSCs populations with regenerative potential equivalent to established MSCs sources, potentially offering new avenues for tissue engineering applications.

2 Material and methods

2.1 Single cell RNA sequencing library preparation and data analysis

This study was approved by the Ethics Committee of the Stomatology Hospital, Zhejiang University School of Medicine, China (No. 2021-11)). Fresh Schneiderian membrane samples from humans were preserved at 4 ℃ with tissue preservation solution. Sequencing was provided by OE Biotech Co., Ltd. (Shanghai, China). Briefly, cellular suspensions were loaded on 10X Genomics Controller single cell sequencer according to the manufacturer's protocol. Single-cell sequencing libraries were then generated by an established protocol using the 10×Genomics Chromium Next GEM Single Cell 3′ Reagent Kits v3.1. FASTQ files were processed and aligned to the GRCh38 human reference genome using Cell Ranger software (version 5.0.0) from 10x Genomics, with unique molecular identifier (UMI) counts summarized for each barcode. The UMI count matrix was then analyzed using Seurat (version 4.0.0) R package. To remove low-quality cells and likely

multiplet captures, the gene-cell-barcode matrix of the samples was log-transformed and filtered based on a set of criteria: cells were filtered by (1) gene numbers (<200), (2) UMI (<1000), (3) lgGenesPerUMI (<0.7), (4) percentage of mitochondrial RNA UMIs (>10%) and (5) percentage of hemoglobin RNA UMIs (>5%). Subsequently, the DoubletFinder package (version 2.0.3) was used to identify potential doublets. To obtain normalized gene expression data, library size normalization was processed using the NormalizeData function.

The top 2000 highly variable genes (HVGs) were identified using the Seurat function Find Variable Genes (mean.function=FastExpMean,dispersion.function=FastLogVMR). Principal-component analysis (PCA) was run on the normalized gene-barcode matrix to reduce the dimensionality. Graph-based clustering was performed using the FindClusters function to cluster cells according to their gene expression profile. Cells were visualized using a 2-dimensional Uniform Manifold Approximation and Projection (UMAP) algorithm with the RunUMAP function. The FindAllMarkers function (test.use=presto) was used to identify marker genes of each cluster. Differentially expressed genes (DEGs) were selected using the function FindMarkers (test.use=presto). $P<0.05$ and |log2foldchange|>0.58 was set as the threshold for significant differential expression.

2.2 Management of Animals

Eighteen male New Zealand white rabbits (mean body weight 3.0 kg) were allocated to five experimental cohorts. Initial protocol validation was performed through terminal anesthesia and tissue harvest (n=1) for baseline histological analysis using hematoxylin and eosin (H&E) staining and Masson's trichrome staining. Comparative phenotypic characterization of BMSCs and SMMSCs was conducted through enzymatic digestion using donor cells from three animals. For cellular tracking studies, three subjects received intramuscular chloromethyl-benzamidodialkylcarbocyanine (CM-Dil) fluorescent dye administration (0.5 g/L; Thermo Fisher Scientific, Waltham, USA). Two animals underwent bilateral maxillary sinus floor elevation procedures with immunohistochemical evaluation. The remaining nine rabbits were subjected to calvarial defect models (4-cm diameter trephination) with subsequent implantation of SMMSCs- or BMSCs-loaded scaffolds, with serial micro-CT scanning at 4/8/12-week endpoints to quantify osteogenic potential. All animal experiments complied with the Animal Research Reporting In Vivo Experiments (ARRIVE) guidelines. Approval for this experiment was obtained from the Animal Care and Use Committee of Zhejiang University, No. ZJU20230115. During the experimental period, the rabbits were kept individually in cages under standard laboratory conditions, with a standard diet and free access to water.

2.3 MSCs isolation, culture, and tri-lineage induction

Briefly, rabbits were anesthetized and euthanized for tissue extraction. Using surface landmarks as a guide, a 3 cm×6 cm area along the nasal septum was shaved. The Schneiderian membrane was retrieved. H&E staining and Masson trichrome staining were done. The Schneiderian membrane was minced and digested with collagenase I (3 mg/mL; Gibco (17100-017), Thermo Fisher Scientific) for 1 h at 37 °C. After neutralization of collagenase, the SMMSCs were collected by centrifugation, re-suspended, and plated onto 10-cm culture dishes. α-minimal essential medium (α-MEM; Hyclone, Cytiva, Marlborough, USA) with 10% (v/v) fetal bovine serum (FBS; Gibco (10099141), Thermo Fisher Scientific), and 1% (v/v) penicillin-streptomycin (Sciencell, Cytiva, Marlborough, USA) was used as a complete medium for cell culture. The medium was changed every other day. BMSCs were also harvested from the same rabbit, as previously described(Saha, et al., 2019). All cell cultures were maintained at 37 °C in 5% CO2. The third passage of cells was used in subsequent experiments.

The experimental sample size was determined through a priori power analysis ($\alpha=0.05$, $\beta=0.2$) to ensure statistical validity of relative standard deviation (RSD) calculations, with triplicate biological replicates (n=3) established as the minimal requirement per experimental group. SMMSCs and BMSCs were isolated from three rabbits by density gradient centrifugation. These autologous cell populations were subsequently subjected to standardized fibroblast colony-forming unit (CFU-F) assays in α-MEM culture medium supplemented with 10% (v/v) FBS. CFU-F assay was conducted on passage 1 (P1) rabbit SMMSCs and BMSCs. Single-cell suspensions were plated at 100 cells/cm² in α-MEM supplemented with 10% (v/v) FBS (Gibco, Thermo Fisher

Scientific). After being cultured for 4 d, colonies were stained with 0.03 g/mL crystal violet.

The multilineage differentiation potential of SMMSCs was analyzed with specific inductive media. SMMSCs from the second passages were seeded in six-well plates at 1×10^4 cells/well until sub-confluence. For osteogenic differentiation, cells were incubated in an osteogenic inductive medium containing 10 mmol/L β-glycerophosphate, 50 μg/mL l-ascorbic acid, and 10 nmol/L dexamethasone (all from Sigma, Merck, St. Louis, USA), and then refreshed every three days. After undergoing osteogenic induction for 21 d, alizarin Red-S (ARS) (Solarbio, Beijing, China) staining was carried out to assess calcium nodes.

For adipogenic differentiation, an adipogenic inductive medium composed of 10 mg/L insulin, 1×10^{-6}mol/L dexamethasone, 0.45 mmol/L isobutyl methylxanthine, and 500 mmol/L indomethacin (all from Sigma) was added and then renewed every 3 d. After 21 days, oil droplets in cells were stained with Oil Red O (Leagene, Beijing, China) solution and observed under a light microscope.

For chondrogenic induction, a chondrogenic inductive medium containing 10 μg/L transforming growth factor (TGF)-β1, 50 μg/mL vitamin C, 1×10^{-8} mol/L dexamethasone, and 1 mmol/L pyruvate (all from Sigma) was added and then renewed every 3 d. After 21 d, cartilage-specific proteoglycan was evaluated by Alcian blue (Solarbio) staining and recorded with photos.

2.4 Immunofluorescence assay

After 21 d of culture growth under multilineage differentiation conditions, cells were fixed with 4%(w/v) paraformaldehyde (PFA) for 15 min, and permeabilized by 0.5% (v/v) Triton X-100 for 10 min. The samples were then blocked with 2%(w/v) BSA for 1 h at room temperature and incubated with osteopontin (OPN, Thermo Fisher, MA5-17180), adiponectin (ADN, Thermo Fisher, MA1-054), and collagen type 2A (COL-II, DSHB, Iowa City, USA, II-II6B3) at 4 °C overnight. Afterward, cells were incubated with fluorescence-conjugated secondary antibody (1:200, v/v) at room temperature for 60 min. Finally, nuclear staining was performed with an anti-fluorescence quencher with DAPI. The stained cells were imaged using confocal fluorescence microscopy (LSM980, Zeiss, Oberkochen, Germany).

Immunohistological staining for Paired Related Homeobox 1 (PRRX1) was performed on 4-μm paraffin sections. Briefly, specimens from human and rabbit were isolated, fixated in 4%(w/v) PFA for 24 h, and decalcified by 10% ethylenediaminetetracetic acid (EDTA, pH 7.4, w/v) for 60 d. Then the tissues were embedded in paraffin and sectioned at 4μm thickness. Heat-induced antigen retrieval was performed, and then the tissue sections were blocked with goat serum. Primary antibody was incubated overnight at 4 ℃ with anti-PRRX1 (LSBio, Seattle, USA, LS-B2380, 1:100, v/v), followed by donkey-anti-goat-Alexa Fluor 488 (Thermo Fisher, A21206, 1:200, v/v) at room temperature for 1 h. Finally, nuclear staining was performed with an anti-fluorescence quencher with DAPI. The tissue sections were imaged using confocal fluorescence microscopy (LSM980, Zeiss).

2.5 Cytoskeleton staining

To assess the growth of cells on GelMA-based scaffolds, 2×10^6 SMMSCs and BMSCs were respectively inoculated on the scaffolds and incubated for 24 h. The cell scaffolds were fixed with 4%(w/v) PFA and permeabilized by 0.5%(v/v) Triton X-100 solution. Next, the cell scaffolds were incubated with rhodamine phalloidin (Cytoskeleton, Denver, USA) in dark conditions for staining the cell cytoskeleton. Subsequently, the cell scaffolds were washed with PBS and stained with DAPI. Fluorescence images were acquired using a laser confocal microscope (LSM980, Zeiss).

2.6 Surgical procedure

2.6.1 Rabbit sinus floor elevation model

Briefly, sodium pentobarbital (30 mg/kg) was intravenously injected to induce general anesthesia. In addition, local anesthesia was provided using 2% (w/v) lidocaine, applied with 1:100 000 (v/v) epinephrine for local hemostasis. The sinus floor elevation (SFE) procedure on both sides was performed(Weng, et al., 2022).

The estimated surgical area was depilated and locally disinfected. A 50-mm mid-sagittal incision was made at the nasal dorsum and a full-thickness flap was elevated. Under continuous refrigeration with 0.9% (w/v) sterile saline solution, two bone windows were made bilaterally with a 4-mm diamond burr (Fig. 1a). The Schneiderian membrane was meticulously elevated using microsurgical instrumentation. Bilateral sinus sites were assigned randomly to either the Bio-Oss® (Geistlich Biomaterials, Wolhusen, Switzerland) collagenated bone mineral group or the 5% gelatin methacrylate (GelMA, ELF, EFL-GM-30, Suzhou, China, w/v) hydrogel treatment group through a split-mouth design. In the left sinus space, Bio-Oss was packed in the new compartment under the elevated sinus membrane. For intraindividual comparison, the right cavity of the same rabbit received 5% (w/v) GelMA-based hydrogels Subsequently, the surgical field was covered by a biodegradable collagen membrane (BioGide, Geistlich Biomaterials). Finally, the periosteum was closed tightly with an absorbable suture type 4-0 and the skin was then sutured with 3-0 silk suture materials. After surgery, all rabbits were medicated with 0.2 ml/kg penicillin for 3 days by intramuscular administration. The rabbits were sacrificed at 6 months or 12 months postoperatively by anesthesia overdose.

2.6.2 Rabbit cranial bone defect model

For the calvarial defect model, a cohort of nine rabbit specimens underwent staggered euthanasia at predetermined postoperative intervals (n=3 per timepoint) to assess temporal variations in bone regeneration outcomes, with terminal endpoints established at 1, 2, and 3 months, respectively. General anesthesia, surgical area disinfection, and local anesthesia were performed in the manner mentioned above. A sagittal midline scalp incision about 4 cm long was performed. To exhibit less individual variation, four circular calvarial defects, each 8 mm in diameter and 2 mm deep, were created in the parietal bones on each side of the median sagittal suture. Circular osseous bony defects were generated using a trephine burr with constant saline irrigation while preserving the underlying dura mate. Computer-generated pseudorandom number sequences were used for stratified randomization of experimental groups. Following surgical creation of osseous defects, the lesion sites were randomly allocated to receive one of four interventions: (1) acellular GelMA-based scaffold implantation, (2) scaffold loaded with 2×10^6 rabbit SMMSCs, (3) scaffold containing 2×10^6 rabbit BMSCs, or (4) negative control group maintaining untreated defects. After the implantation of the materials, a barrier membrane (BioGide, Geistlich Biomaterials) was used to cover the defect site. The periosteum and skin were closed in layers using 4–0 Vicryl. The rabbits also received intramuscular injections of penicillin (0.2 mg/kg) for up to 3 d for postoperative care.

2.7 CM-Dil tissue-labeling

Chloromethyl-benzamidodialkylcarbocyanine (CM-Dil) tissue-labeling was applied as described(Yuan et al., 2020). CM-Dil (Molecular Probes CellTracker CM-DiI, C-7000, Sigma) at 1 g/L in 100% ethanol was diluted to 0.5 g/L with α-MEM medium containing 10%(v/v) FBS. The Dil solution was carefully injected at the elevated Schneiderian membrane using micropipettes, to monitor the contribution of the Schneiderian membrane. 5%(w/v) GelMA-based hydrogel was then packed under the elevated sinus membrane. The rabbits were sacrificed separately at 0, 4 and 8 weeks after surgery. The tissues were fixed with 4%(w/v) PFA, decalcified, embedded in Tissue-Tec O.C.T. compound (Sakura Finetek, Tokyo, Japan) and then cut into sections (8 um). Fluorescence images were taken using a laser confocal microscope (LSM980, Zeiss).

2.8 Micro-CT scanning

Bone samples were dissected and fixed in 4%(w/v) PFA immediately. Specimens were scanned with a local micro-CT (Milabs, Utrecht, Netherlands, U-CT-XUHR) using the following settings: scan energy 55 kV, intensity 455 μA, and pixel resolution 14.8 μm using an aluminum filter (0.5 mm). Three-dimensional images of regenerated bone were reconstructed and the total defect volume was considered as the region of interest (ROI). The osteoporosis-based measurements for the ROI were manually determined with reconstruction software (Imalytics Preclinical 2.1) with parameters including bone volume/total volume (BV/TV), trabecular thickness (Tb.Th), and trabecular spacing (Tb.Sp).

2.9 Histological observation

After micro-CT examination, the specimens were cut, decalcified in 10%(w/v) EDTA, dehydrated, embedded in paraffin, and sliced coronally into serial sections of 5 μm thickness. For immunohistochemistry analysis of bone repair, histological sections were prepared for H&E staining. Samples were subsequently examined for newly formed bone and soft tissue changes and photographed under a light microscope. ImageJ was used to analyze the bone area ratio(Guo et al., 2023).

2.10 Statistical analysis

Statistical analysis was carried out using one-way ANOVA through SPSS version 19.0 software (IBM Corp., Chicago, USA) for more than two groups. A two-tailed Student's unpaired t-test was used for two-group comparisons. $P < 0.05$ was considered statistically significant. Differences between groups are expressed as mean ± standard deviations.

3 Results

All rabbits recovered from anesthesia and the surgical procedure, and the sutures healed well. The rabbits did not show any signs of inflammation or infection by the time of sacrifice.

3.1 Schneiderian Membrane Osteogenic Potential in Sinus Augmentation Models

Representative images of the rabbit sinus floor elevation model are shown in Fig. 1a. CM-Dil was further used to trace cells from the rabbit Schneiderian membrane and their progeny to identify the contribution of the membrane to bone regeneration (Fig. 1b). After 4 weeks, labeled cells underwent proliferation and increased significantly. After 8 weeks, Dil-labeled cells gradually became widely distributed in the elevated region. Cells from the maxillary sinus membrane migrated, proliferated, and may have finally differentiated into osteogenic lineages in the elevated area. In the H&E-stained decalcified sample sections (Fig. 1c), new bone was repositioned near the elevated sinus membrane after a long period in two groups. We found that in the 6th month, the Bio-Oss group showed early calcified bone formation in the upper transplantation area near the Schneiderian membrane and around the bone graft material. In the GelMA hydrogel group, calcified tissue was scattered near the Schneiderian membrane and at the edge of the transplantation area. After 12 months of transplantation, a large amount of new bone tissue was formed near the Schneiderian membrane in both the Bio-Oss and GelMA hydrogel groups with a further calcified portion. Active osteoblast aggregation was observed under the Schneiderian membrane, which indicated that the membrane may have long-term bone-inducing potential. Taking these findings together, our data suggested that the maxillary sinus membrane may directly participate in de-novo bone regeneration in the rabbit maxillary sinus augmentation model.

The morphological observations revealed that the rabbit Schneiderian membrane was composed of three layers: the epithelium, lamina propria and periosteum (Fig. S1a and S1b). The upper cortex was composed of a false multilayered epithelium with a neatly arranged ciliated structure. The lamina propria layer was rich in maxillary sinus glands and collagen fibers, and the periosteum layer was closely connected with the bone wall. A recent study suggested that the lamina propria layer and the periosteum layer of the human Schneiderian membrane contained two types of MSCs(Lv, et al., 2024), which may explain the osteogenic potential of the Schneiderian membrane.

3.2 Identification of SMMSCs by scRNA-seq

To identify the cell subsets, distinct populations were identified, including 1 cluster for mesenchymal cells, 5 clusters for globose basal cells, 3 clusters for airway basal cells, 1 cluster for endothelial cells, 2 clusters for secretory goblet cells, 6 clusters for ciliated cells, 1 cluster for monocytes and 1 cluster for lymphocytes (Figs. 2a and 2b). Briefly, globose basal cells expressed *KHDRBS2*, *TP63*, and *TMTC1*, while endothelial cells

showed specific expression of *EMCN*, *VMF* and *LDB2*. Significantly elevated levels of *AL139815.1*, *CFAP157*, and *AC137810.1* were used to distinguish the ciliated cells, and the expression levels of *RIMS1*, *LSAMP* and AC092691.1 were used to distinguish secretory goblet cells. Monocytes and lymphocytes expressed high levels of *ELMO1*, *ARHGAP15*, *PTPRC*, and AC079793.1. Mesenchymal cells showed high levels of *PRRX1*, *ZEB1*,

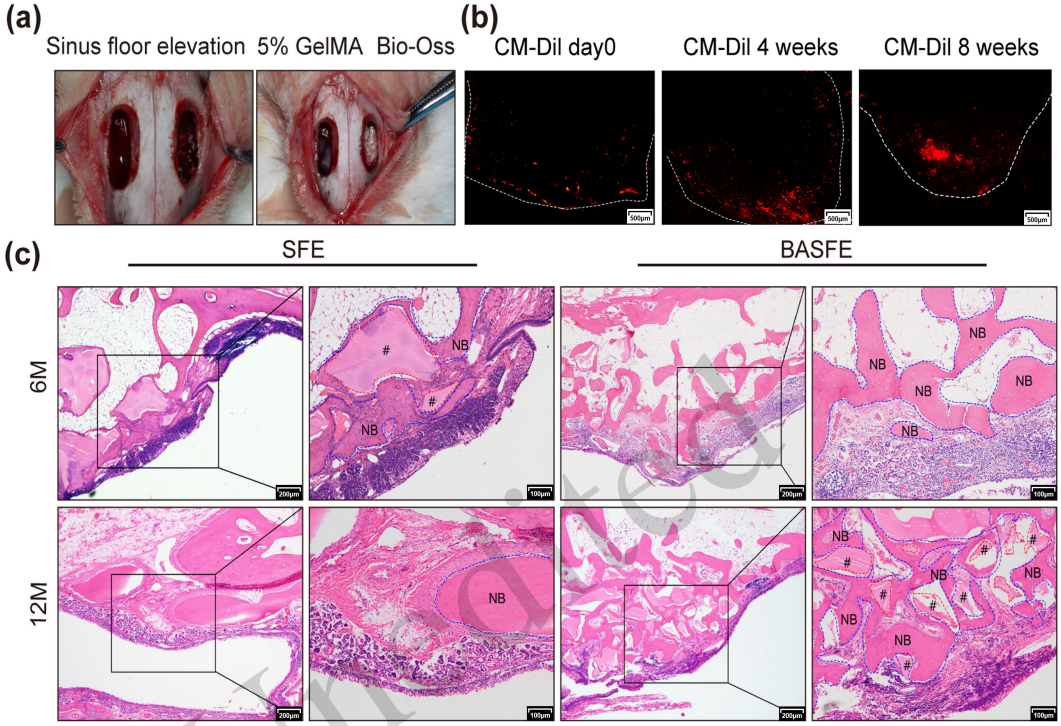

Fig. 1 Schneiderian membrane participated in endo-sinus bone formation in the rabbit sinus floor elevation model. (a) The procedure of rabbit sinus floor elevation. The bony windows obtained by surgery; frontal view. Elevated spaces of the two sinuses were filled with Bio-Oss and 5% gelatin methacrylate (GelMA)-based hydrogels, respectively; frontal view. (b) CM-Dil was used to evaluate the contribution of the Schneiderian membrane to endo-sinus bone formation. With the extension of tracing time, cells derived from the Schneiderian membrane gradually proliferated. The dotted lines mark the elevated Schneiderian membrane, below which is the maxillary sinus cavity. (c)Representative histological images of Hematoxylin and eosin(H&E) staining at 6 months (6M) and 12 months (12M) of two groups are shown. The new bone was located near the elevated Schneiderian membrane. The right image of each pair shows a magnified rectangular region of the left image. The blue dotted lines mark new bone (NB), and the red dotted lines and "#" mark unabsorbed grafting materials. SFE, sinus floor elevation, BASFE, bone added sinus floor elevation.

and *NAV3*. We further observed that cluster 9 was highly enriched in the previously reported mesenchymal marker *PRRX1* (Fig. 2c). Specifically, *PRRX1* was also identified as classical MSCs marker in the maxillofacial region. We found that *PRRX1*$^+$MSCs could be divided into 5 subclusters (Fig. S2a and S2b). Besides, the pseudotime differentiation trajectory (Fig. S2c) indicated that different *PRRX1*$^+$MSCs subclusters may have different osteogenic differentiation capacities.

Through immunofluorescence (IF) staining, we further revealed the localization of *PRRX1*$^+$ cells in human and rabbit Schneiderian membranes. As shown in Fig. 2d and e, *PRRX1*$^+$cells were scattered in the lamina propria layer in both human and rabbit Schneiderian membranes, close to the periosteum layer. After sinus floor elevation for 4 weeks, *PRRX1*$^+$cells proliferated and participated in the early-stage of new bone formation (Fig. 2f). After 8 weeks, more *PRRX1*$^+$cells appeared in the elevated zone, suggesting that *PRRX1*$^+$cells may further promote bone regeneration (Fig. 2g). Building upon integrative analysis of single-cell RNA sequencing and spatially resolved immunofluorescence staining data, our findings suggested that *PRRX1*-positive cell populations localized within both the lamina propria and periosteal compartments could represent progenitor lineages potentially associated with endo-sinus osteogenic processes.

3.3 Characterization and differentiation potential of rabbit SMMSCs

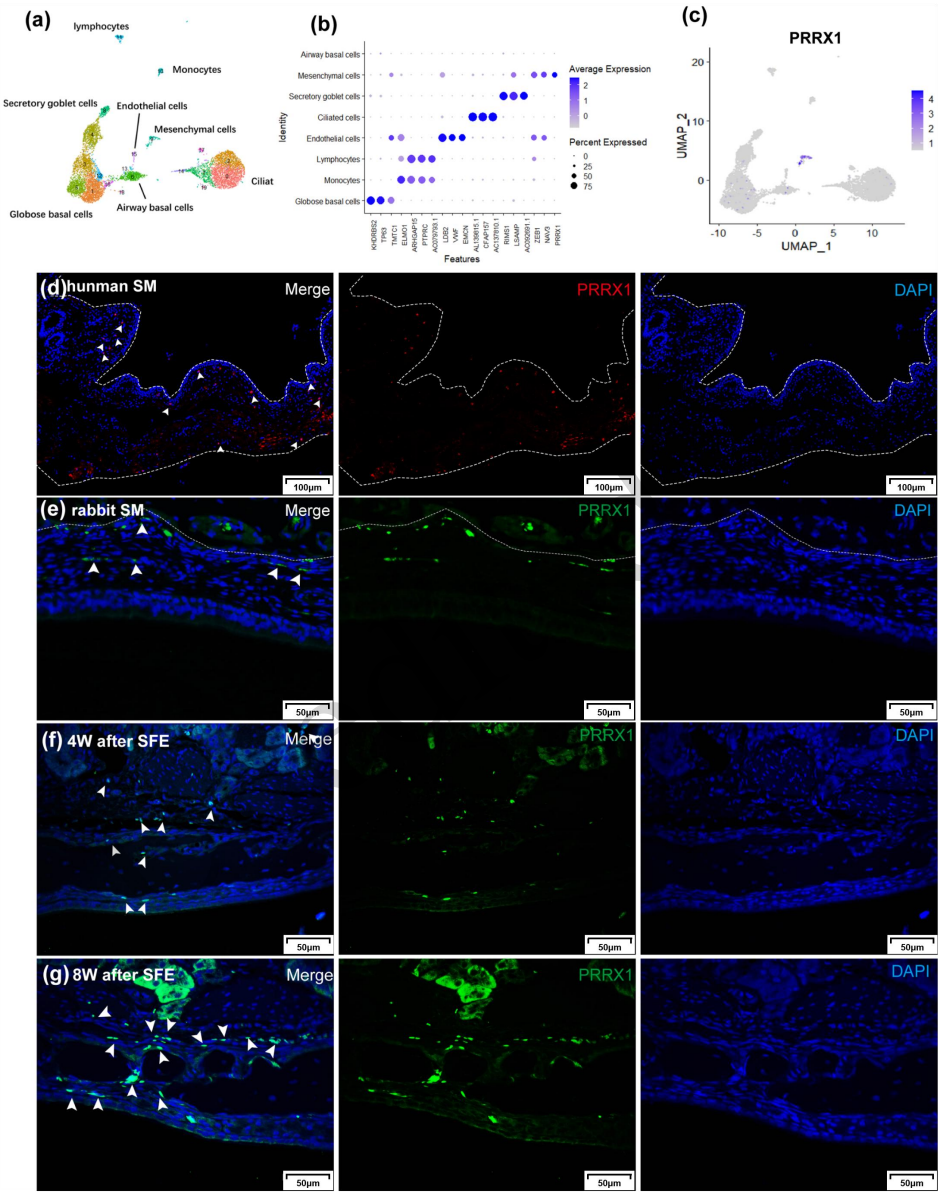

Fig. 2 Features of paired related homeobox1 (*PRRX1*$^+$) cells in the Schneiderian membrane. (a) A transcriptomic map of cells in the human maxillary sinus membrane was produced by single cell RNA sequencing (scRNA-seq). Cell type annotations of distinct clusters are shown. (b) The dot plot displays the average expression levels of key markers for different types of cells, as well as the percentage of cells expressing each marker. (c) A Uniform Manifold Approximation and Projection (UMAP) plot of mesenchymal cells is shown according to their marker gene *PRRX1*. (d) *PRRX1*$^+$cells were determined by immunofluorescent staining in the human Schneiderian membrane (SM). The dotted lines mark the Schneiderian membrane and the maxillary bone. The arrows mark the *PRRX1*$^+$cells in the human Schneiderian membrane. (e) *PRRX1*$^+$ cells were distinguished by immunofluorescent staining in the rabbit Schneiderian membrane (SM). The dotted lines mark the Schneiderian membrane, above which is the maxillary bone. The arrows mark the *PRRX1*$^+$ cells in the rabbit Schneiderian membrane. (f, g) *PRRX1*$^+$cells were identified by immunofluorescent staining after sinus floor elevation at 4 weeks (4w) and 8 weeks (8w). The arrows mark the PRRX1+ cells in the new bone.

Primary cultured SMMSCs showed spindle-shaped fibroblast-like morphology, similar to the cultures of MSCs derived from other tissues (Fig. 3a). A CFU-F assay was conducted on P1 rabbit SMMSCs and BMSCs to identify their self-renewal ability. Fig. 3b shows representative colonies after cultivating rabbit SMMSCs and

BMSCs for 2 days. SMMSCs showed significantly higher self-renewal ability than BMSCs (*$P < 0.05$).

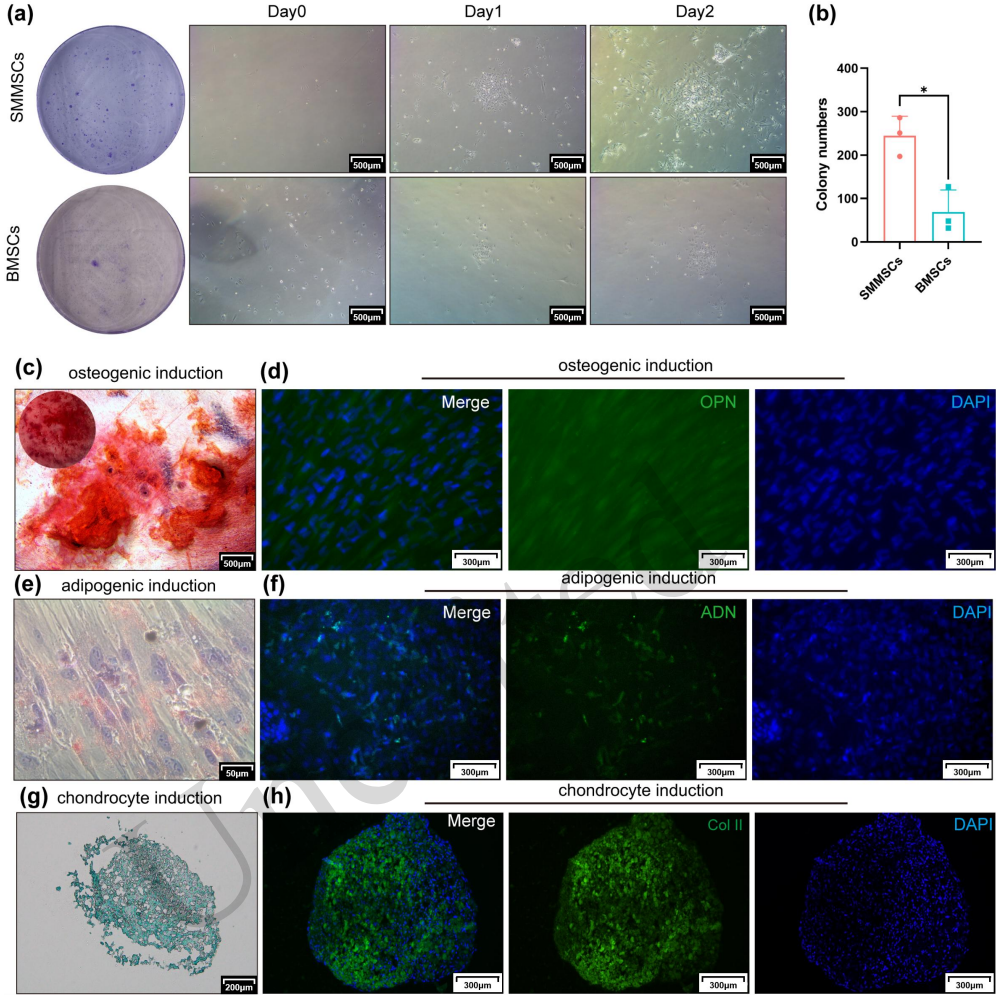

Fig. 3 Characterization of rabbit Schneiderian membrane-derived mesenchymal stem cells (SMMSCs). (a) Representative images of fibroblast colony-forming units (CFU-F) after cultivating rabbit SMMSCs and bone marrow-derived mesenchymal stem cells (BMSCs) for 2 d under inverted microscopy. (b) SMMSCs showed better self-renewal ability than BMSCs (*P<0.05, two-tailed Student's unpaired t-test, n=3). (c) Representative images of Alizarin Red S staining for rabbit SMMSCs osteogenic differentiation. (d) Osteopontin (OPN) was determined by immunofluorescent staining. (e) Adipogenic rabbit SMMSCs were stained by Oil Red O. (f) Adiponectin (ADN) was revealed by immunofluorescent staining. (g) Chondrogenic rabbit SMMSCs were stained by Alcian blue. (h) Collagen type 2A (COL-II) was identified by immunofluorescent staining.

The capacity of rabbit SMMSCs to differentiate into osteogenic, adipogenic, and chondrogenic cells was investigated under in vitro conditions. For osteogenic differentiation, Alizarin Red S staining revealed rabbit SMMSCs differentiated into osteoblasts after 21 days of induction (Fig. 3c). These observations were supported by positive OPN staining detected in osteogenic rabbit SMMSCs. Adipogenic SMMSCs were stained with Oil red O to assess lipid droplets (Fig. 3e). The adipogenic marker ADN evaluated by immunofluorescence was significantly upregulated in adipogenic SMMSCs (Fig. 3f). For chondrogenic differentiation, the pellet cultures stained by Alcian Blue revealed that chondrogenic rabbit SMMSCs increased after 21 days of chondrogenic induction (Fig. 3g). The immunofluorescence experiment also showed that COL-II significantly increased in chondrogenic rabbit SMMSCs (Fig. 3h). Taken together, these results showed that rabbit SMMSCs had a better self-renewal capability than BMSCs, and had the potential to form osteogenic, adipogenic, and chondrogenic lineage cells.

3.4 Osteogenic potential of rabbit SMMSCs in cranial defect repair

Cytoskeleton staining indicated that the GelMA-based scaffold supported the expansion of SMMSCs and BMSCs (Fig. 4a). Representative images of the rabbit cranial bone defect model are shown in Fig. 4b. Fig. 4c depicts micro-CT 3D images of cranial bone defects taken at 1 month, 2 months, and 3 months following: no treatment; implantation with GelMA-based scaffolds only; rabbit SMMSCs/ GelMA-based scaffolds; rabbit BMSCs/ GelMA-based scaffolds. At one month postoperatively, new bone formation was clearly observed at the edge and center of the cranial defects in the SMMSCs and BMSCs groups, while only a small amount of new bone formation was observed at the edge of the cranial defect in the blank control group and the GelMA group. The bone volume fraction (BV/TV) was significantly higher in the SMMSCs/ GelMA-based scaffold group than in the BMSCs/ GelMA-based scaffold group (P<0.01), GelMA-based scaffold group (P<0.001) or the blank group (P<0.01). In addition, the trabecular thickness (Tb.Th) of new bone in the SMMSCs/ GelMA-based scaffold group was significantly higher than that in GelMA-based scaffold group *(*P<0.01) or the blank group (P<0.001). These results indicated that SMMSCs had better bone defect repair capacity at an early stage than BMSCs.

As time progressed, the percentage of new bone formation increased in all groups. After two months, the SMMSCs and BMSCs/ GelMA-based scaffold groups had mostly repaired the bone defect. At this time, a large defect was still visible in the center of the cranial bone in the GelMA-based scaffold and the blank groups. After two months, the BV/TV in the SMMSCs/ GelMA-based scaffold group was significantly higher than that in GelMA-based scaffold group (P<0.5), and the BV/TV in the BMSCs/ GelMA-based scaffold group was also significantly higher than that in the GelMA group (P<0.01). The considerable new bone formation in SMMSCs/ GelMA-based scaffold and BMSCs/ GelMA-based scaffold groups had mostly repaired the defect, while in contrast, GelMA-based scaffolds and empty control groups showed only a slight increase in newly formed bone. The bone defect had mostly healed in all groups after three months. After three months, the BV/TV in the BMSCs/ GelMA-based scaffold group was significantly higher than that in GelMA-based scaffold group (P<0.01) and blank group (P<0.01), and Tb.Th in the BMSCs/ GelMA-based scaffold group was significantly higher than that in blank group (P<0.5). These results indicate that both SMMSCs and BMSCs have good bone repair ability, and SMMSCs may have better in vivo osteogenic ability than BMSCs at an early postoperative stage.

H&E staining of the cranial bone defects is shown in Fig. 5. After 1 month, in the GelMA-based scaffold and empty control groups, the center of defect sites was filled mostly with connective tissue rather than newly formed bone. Only minimal bone formation and a few bony islands were noted on the edge of the defects. On the other hand, MSCs-treated groups showed considerable new bone formation: circular new bony islands with early woven bone were observed, originating from the periphery of defects. The SMMSCs/ GelMA-based scaffold group formed more continuous fibrous osteoid structures and bone marrow cavities, with a large number of osteoblasts and new bony islands.

After 2 months of healing, amounts of bony ingrowth were observed and bone maturation was more extensive in MSCs-treated groups. Mature continuous lamellar bone as well as bone marrow cavities were noted in the SMMSCs/ GelMA-based scaffold and BMMSCs/ GelMA-based scaffold groups, while new bone formation was still limited in the blank group and the GelMA control group, with a limited number of independent bone islands or discontinuous thin fibroid bone. After 3 months, robust bone regeneration and defect healing were clearly observed in the defects implanted with SMMSCs and BMSCs. The rabbit cranium defect area was covered with thick mature lamellar bone junctions with large and orderly trabeculae in the SMMSCs/ GelMA-based scaffold and BMSCs/ GelMA-based scaffold groups. In contrast, the blank group and the GelMA control group formed isolated bone islands surrounded by fibrous tissue, with thin bone and small trabeculae.

A semiquantitative analysis of the bone formation in the cranial bone defects suggested that SMMSCs exhibited the highest healing speeds during the entire bone healing process. After 1 month, the proportion of new bone in the SMMSCs/ GelMA-based scaffold group was significantly higher than that of the BMSCs/

GelMA-based scaffold group (*P < 0.05), GelMA-based scaffold group (****P < 0.0001) and blank group

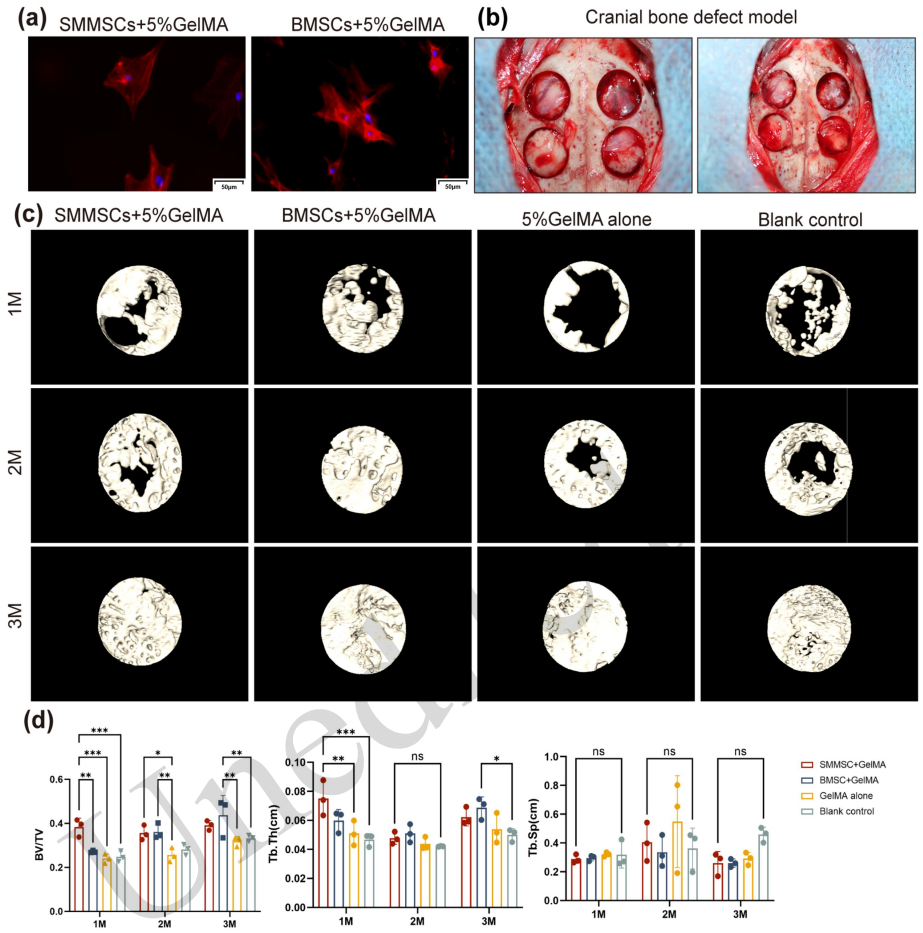

Fig. 4 Micro-CT suggested earlier bone formation by SMMSCs relative to BMSCs in calvarial defects. (a) Cytoskeleton staining was used to observe the growth of rabbit SMMSCs and BMSCs on GelMA-based scaffolds. (b) Rabbit cranial bone defect model, frontal view. (c) Representative 3D micro-CT images of a top view of the reconstructed rabbit calvaria at 1 month (1M), 2 months (2M), and 3 months (3M). Remarkable new bone formation was observed in the SMMSCs/ GelMA-based scaffold group and the BMSCs/ GelMA-based scaffold group at 1 month after surgery. (d) Morphometric analysis of bone volume/total volume (BV/TV), trabecular thickness (Tb.Th, mm), and trabecular spacing (Tb.Sp, mm) within the calvarial defects at 1M, 2M, and 3M for different groups. After 1 month, the BV/TV in the SMMSCs/ GelMA-based scaffold group was significantly higher than that in the BMSCs/ GelMA-based scaffold group (P<0.01), the GelMA-based scaffold group (***P<0.001) and the blank group (***P<0.001). ANOVA, followed by Tukey's post hoc test. ns, not significant. n=3.**

(***P < 0.001). The proportion of new bone in the BMSCs / GelMA-based scaffold group was significantly higher than that in the GelMA-based scaffold group (***P< 0.001) and the blank group (*P < 0.05). After 2 and 3 months, both SMMSCs and BMSCs significantly enhanced bone regeneration in the cranial bone defects model when compared with GelMA alone or the blank control (**P< 0.01, ***P < 0.001, ****P < 0.0001). These results suggest that both SMMSCs and BMSCs had the ability for bone regeneration in vivo, and that SMMSCs may have better osteogenic ability than BMSCs at 1 month after surgery.

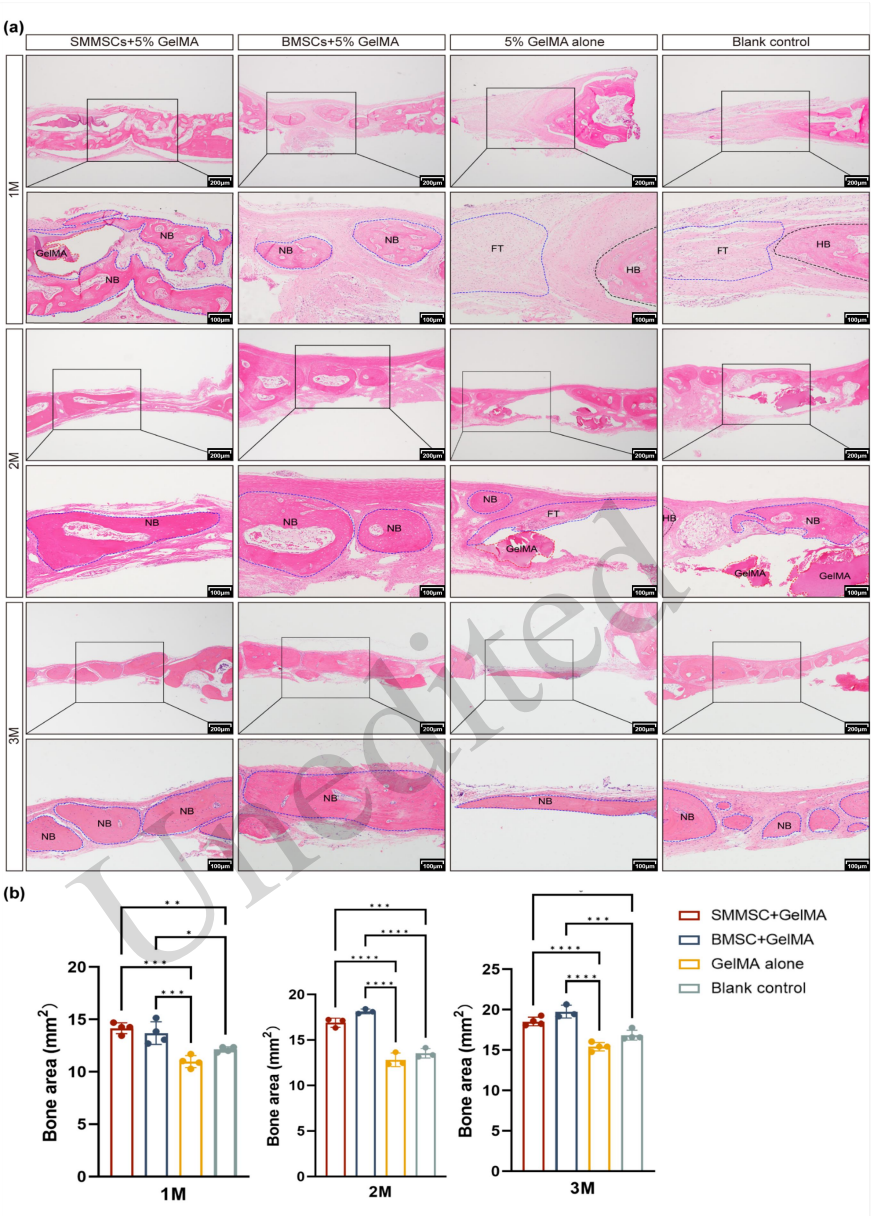

Fig. 5 Histomorphological detection indicated accelerated osteogenesis of SMMSCs versus BMSCs during early-stage calvarial healing. (a) Histomorphological detection was demonstrated by H&E staining. Continuous new bone formation was detected in the SMMSCs and BMSCs/ GelMA-based scaffold groups at different periods after surgery. The lower image in each set shows a magnified rectangular region of the upper image. The blue dotted lines mark the new bone (NB) and fibrous tissue (FT), the red dotted lines mark unabsorbed GelMA materials, and the black dotted lines mark the host bone (HB). (b) ImageJ was used to measure the bone formation area of each treatment group on the H&E stained slides. The new bone proportion in the SMMSCs/ GelMA-based scaffold group was significantly higher than those of the BMSCs / GelMA-based scaffold group (*P<0.05), GelMA-based scaffold group (**P<0.0001) and blank group (***P<0.001) at one month. ANOVA, followed by Tukey's post hoc test. n=3.**

4 Discussion

Vertical bone regeneration in the maxillary posterior alveolar ridge remains a significant clinical challenge for successful dental implant placement. Maxillary sinus elevation is usually performed in these cases. There is controversy regarding the underlying mechanism of osteogenesis in the maxillary sinus cavity. Previous studies

suggested that bone regeneration after maxillary sinus floor elevation relied mainly on the activation of osteoprogenitor cells located in the maxillary bone wall and bone marrow(Scala et al., 2012; Jungner et al., 2015; Qian et al., 2018). In recent years, the Schneiderian membrane, which covers the maxillary sinus cavity, has attracted attention from scholars for inducing regenerative tissues. Guo et al. proposed that the Schneiderian membrane was one of the sources of osteoblasts involved in the endo-sinus bone remodeling process(Guo, et al., 2015). Srouji et al. showed that when the sinus membrane is folded and transplanted in an ectopic subcutaneous location in nude mice, strong positive staining of ALP appeared at the periosteum-like structure(Srouji et al., 2010). Weng et al. showed that *Krt14*$^{+}$*Ctsk*$^{+}$ cells in the Schneiderian membrane contributed to maxillofacial bone osteogenesis and regeneration through dual recombinase-mediated lineage tracing(Weng, et al., 2022). However, Scala et al. found no evidence that the Schneiderian membrane participated in new bone formation after maxillary sinus floor elevation in histological sections of primates(Scala, et al., 2012). Lim et al. documented the early degradation of pseudo-periosteal structures during wound healing, postulating a limited osteogenic contribution from the sinus mucosa(Lim et al., 2022). This observation aligned with retrospective clinical evidence demonstrating enlargement of the maxillary sinus ostium post-augmentation(Guo, et al., 2015; Makary et al., 2016; Sakuma et al., 2020), suggesting that chronic inflammatory processes and sustained edema may adversely affect neo-osteogenesis. Therefore, the mechanistic role of the sinus mucosa in endo-sinus osteogenesis warrants further experimental validation through integrated in situ cell lineage tagging and histomorphometric validation.

In the present animal experiments, we performed maxillary sinus augmentation with Bio-Oss or GelMA hydrogel in rabbits for long-term observation. Bio-Oss is a standard commercial bone graft substitute for maxillary sinus floor augmentation(Pereira et al., 2024), and GelMA hydrogel has good biocompatibility and provides structural support(Chen and Tsai, 2025; Liu et al., 2025). After 6 months, both Bio-Oss materials and GelMA hydrogel were retained in the rabbit sinus as they could be seen clearly in H&E stained slides. At 12 months post-surgery, GelMA hydrogel in the rabbit sinus had been resorbed to some extent and replaced by vital bone. In-growth of newly formed bone could be found around the implantation materials in both groups. Our results showed that the elevated Schneiderian membrane was in intimate contact with the new bone after a long period of time. To further explain the unique function of the sinus mucosa in the endo-sinus bone gain, CM-Dil tracing was used to track the Schneiderian membrane-derived cells after sinus elevation. The labeled cells proliferated and scattered in the maxillary sinus cavity in postoperative week 4 and week 8. We hypothesize that the de novo bone generated from the Schneiderian membrane may exhibit distinct histomorphometric characteristics, particularly in its preferential deposition along the arcuate superior region of the sinus compartment. This osteogenic pattern potentially diverges from the intramembranous ossification processes originating from the maxillary bony walls. The results indicated that the Schneiderian membrane-derived cells directly participated in bone gain after sinus lifting.

H&E and Masson trichrome stained sections showed that the Schneiderian membrane was composed of the epithelial lining, lamina propria, and a periosteum-like structure. After the sinus membrane is elevated, the osteoprogenitor cells may be stimulated to start the osteogenesis process. Meanwhile, as a barrier membrane, the Schneiderian membrane could also protect the blood clot in the raised space, thereby contributing to the osteogenic response(Falah et al., 2016).

The cellular composition of the Schneiderian membrane is not well understood. Therefore, we conducted single-cell RNA sequencing to explain the contribution of the Schneiderian membrane and identify the MSCs residing within it. We determined the cellular hierarchy of the maxillary sinus membrane and identified specifically labeled MSCs. The human maxillary sinus membrane contains mesenchymal cells, globose basal cells, airway basal cells, endothelial cells, secretory goblet cells, ciliated cells, monocytes, and lymphocytes. In recent years, three distinct cell markers have been used to identify MSCs and skeletal stem cells in the craniofacial region, including *PRRX1*(Tooze et al., 2023), GLI family zinc finger 1 (*GLI1*)(Yu et al., 2021), and axis inhibition protein 2 (*AXIN2*)(Di Pietro et al., 2020). *PRRX1*, which acts as a transcriptional co-activator, has been shown to be expressed within periosteal bone(Deng et al., 2019; Yang et al., 2022). *GLI1*$^{+}$ cells seem to

be involved in cranial suture regeneration and bone homeostasis(Zhao et al., 2015; Yu, et al., 2021). Finally, *AXIN2*$^+$ cells have been proposed to have long-term self-renewal and differentiation abilities during calvarial development(Maruyama et al., 2017). *PRRX1*, a lineage-specific subset of craniofacial mesenchyme progenitors, appears to contain osteoprogenitors in both human and rabbit Schneiderian membranes. After sinus floor elevation, *PRRX1*$^+$ MSCs scattered in both the lamina propria and periosteum layers were considered to play an important role in guiding bone regeneration. Once the sinus membrane was lifted, *PRRX1*$^+$ cells were enriched and located in the newly-formed bone, suggesting that they contributed to the development of newly formed bone tissue. Interestingly, *PRRX1*$^+$ MSCs could be further divided into five subpopulations, with pseudotime analyses showing their differentiation trajectory. The heterogeneity and hierarchy of *PRRX1*$^+$ MSCs subpopulations that participate in endo-sinus bone regeneration and their specific function will be verified in further studies. While preliminary findings suggest *PRRX1*$^+$ SMMSCs involvement in sinus bone formation, the current study had limitations in conclusively demonstrating cellular dynamics and commitment pathways. Definitive validation requires implementation of Cre-loxP-based lineage tracing in transgenic models coupled with single-cell transcriptomic profiling, which may permit high-resolution tracking of *PRRX1*$^+$ progenitor differentiation trajectories during osteogenic processes.

Numerous MSCs from different tissues have been extensively applied in cell therapies(Granchi, et al., 2010; Lemos, et al., 2015; Fujii, et al., 2023). Cells isolated from various sources exhibit different biological characteristics(Sui et al., 2019). In particular, the bone marrow stromal cells and periosteum-derived cells have been the main sources used in bone repair and tissue engineering(Zhu et al., 2023). In the present study, SMMSCs fostered a fibroblast-like appearance. The colony-forming potential is one of the most essential characteristics of MSCs(Friedenstein et al., 1970). Our results showed that the self-renewal ability of SMMSCs was distinctly higher than that of BMSCs. In addition, MSCs are known for their capacity to differentiate in multi-lineages toward osteoblasts, adipocytes, and chondroblasts(Suchanecka et al., 2025). The multilineage differentiation potential of SMMSCs was proven by the positive staining of Alizarin Red S, Oil Red O, and Alcian blue as well as the elevated lineage-specific expression level including OPN, ADN, and COL-II. Other researchers also derived MSCs from the human Schneiderian membrane that were committed to the osteogenic lineage(Guo, et al., 2015). Some research groups have provided evidence that SMMSCs express the stem cell marker *STRO-1* and the microvascular mesenchymal progenitor marker *CD146*, reconfirming the presence of a progenitor cell population in the Schneiderian membrane(Derjac-Arama et al., 2015; Guo, et al., 2015).

Hence, SMMSCs are a population of MSCs with high self-renewal capability and multi-lineage differentiation potential, which may exhibit significant effects in tissue-engineered bone formation after maxillary sinus floor augmentation. These results emphasize the high bone regeneration potential of MSCs derived from the Schneiderian membrane and raise the possibility of their use in an MSCs-based therapeutic therapy against bone defects in vivo.

The cranial bone defect model has been widely used to investigate the effects of different MSCs-based treatment modalities(Saha, et al., 2019; Liu, et al., 2020). By placing collagen membranes as barriers, we prevented the in-growth of fibrous connective tissues during the healing process, thus the transplant cell-based scaffolds were the main source of bone regeneration(Maurer et al., 2018). With high osteogenic potential, BMSCs have been widely used in many tissue engineering studies(Granchi, et al., 2010; Xie, et al., 2022; Lee, et al., 2023). Thus, we used BMSCs as a control to evaluate the bone regeneration potential of SMMSCs. We observed active new bone formation as well as osteoid/ossifying mesenchyme in SMMSCs/ GelMA-based scaffolds in the first 4 weeks of healing. On the other hand, only small amounts of new bony islands were observed in BMSCs/ GelMA-based scaffolds. Note that we found significantly higher BV/TV values in the SMMSCs/ GelMA-based scaffold group than in the BMSCs/ GelMA-based scaffold group. The other two groups promoted only minimal new bone in the margin area, as the center of the defect regions was filled with connective tissues but not trabecular bone. At 8 weeks, both the BMSCs/ GelMA-based and the SMMSCs/ GelMA-based scaffold groups showed well-organized matured bone with marrow space filled with fat cells. Continuous cortical bone was observed in all four groups after 12 weeks. Compared with control groups,

MSCs-treated groups showed a better degree of mineralization and thicker cortical bone. In conclusion, the results of the present study suggest that more pronounced bone formation occurred in the SMMSCs/ GelMA-based scaffold group in the early healing stage beyond 4 weeks. SMMSCs may have superior osteogenic differentiation and mineralization abilities than BMSCs during the initial period of bone healing in vivo. To reduce individual differences, we did not use a critical calvarial defect model in rabbits, thus caution is necessary when considering the statistical results. To our knowledge, this is the first study to evaluate the in vivo osteogenesis efficacy of SMMSCs in a rabbit calvarial defect model. When compared with autografts, allografts, and xenografts for bone regeneration, allogeneic SMMSCs may have several advantages. This strategy could reduce the risk of immune rejection(Reinders et al., 2013; Ankrum et al., 2014; Chen et al., 2021) and SMMSCs could be minimally invasive isolated in SFE model. The comparative analysis revealed a paradoxical temporal divergence in osteogenic efficacy between SMMSCs and BMSCs, with SMMSCs showing superior early-stage osteoinductive capacity in the cranial defect model. This differential performance profile likely stems from intrinsic cellular adaptations to their respective tissue niches. The observed spatial patterning of de novo bone formation, particularly the peripheral-to-central mineralization gradient in augmented sinuses, may align with the demonstrated propensity of SMMSCs for early bone regeneration. We hypothesize that as mucosal-derived cells subjected to cyclic respiratory deformation, SMMSCs may have enhanced capacity to transduce compressive stresses into pro-osteogenic biochemical signals after SFE.

This study's conclusions must be interpreted with regard to its methodological constraints. Although CM-Dil tracing indicated maxillary sinus membrane involvement in osteogenesis within the rabbit model, direct clinical extrapolation remained problematic due to significant anatomical and physiological disparities in Schneiderian membrane morphology and sinus augmentation dynamics between the species. Moreover, the distinct biological microenvironment of calvarial defects compared to sinus elevation sites underscored the need for caution when translating these findings to maxillofacial regeneration scenarios. Further investigations using human-derived models and clinical correlation studies are imperative to elucidate the role of SMMSCs' in human sinus floor elevation.

In this perspective, endo-sinus new bone formation may promote the participation of the Schneiderian membrane in bone formation. Our study provides initial experimental evidence that the addition of the SMMSCs transplant resembles a biologically active osteoinductive augmentation method which may enhance new bone formation, especially in early bone healing. The demonstrated self-renewal capacity and multipotent differentiation potential of SMMSCs, particularly their osteogenic competency in both in vitro and in vivo models, position these cells as promising candidates for MSCs-based regenerative approaches. To advance clinical translation, ongoing investigations focused on three critical aspects are currently underway: 1) ontogenetic characterization of SMMSCs subpopulations, 2) mechanistic studies of their paracrine signaling in three-dimensional sinus augmentation environments, and 3) development of human-relevant experimental models to validate their osteoinductive capacity in maxillofacial regeneration scenarios.

5 Conclusions

Histological and immunohistochemical evidence suggested the Schneiderian membrane may act as a cellular reservoir supporting osseointegration post-sinus augmentation, though definitive validation via lineage-tracing and spatial transcriptomics is needed. SMMSCs transplantation enhanced earlier calvarial bone regeneration compared to BMSCs. Given their robust self-renewal and osteogenic potential in vitro and in vivo, SMMSCs may represent promising MSCs-based therapeutic candidates for bone repair. Further investigations into their cellular origins and heterogeneity are underway.

Data availability statement

All data supporting the conclusions of the present study are included within this article.

Acknowledgments

This work was supported by the National Key Research and Development Program of China (No. 2023YFB3813003), Innovative Talent of Zhejiang Provincial Health Commission, The Research and Development Project of Stomatology Hospital Zhejiang University School of Medicine (RD2023DLYB02), and National Natural Science Foundation of China (No. 82430031).

Author contributions

Yuxin ZHAO, performed the experiments, analyzed the data, drafted and revised the manuscript; Jia WANG, performed the experiments, drafted and revised the manuscript; Dongqi YOU, participated in the experiments; Yifan LU, interpreted the data and prepared parts of figures; Mengfei YU and Misi SI, designed and supervised this study, critically revised the manuscript. All authors have read and approved the final manuscript, and therefore, have full access to all the data in the study and take responsibility for the integrity and security of the data.

Compliance with ethics guidelines

Yuxin ZHAO, Jia WANG, Dongqi YOU, Yifan LU, Mengfei YU and Misi SI declare that they have no conflict of interest.

All procedures followed were in accordance with the ethical standards of the responsible committee on human experimentation (institutional and national) and with the Helsinki Declaration of 1975, as revised in 2008. Informed consent was obtained from all patients for being included in the study. Additional informed consent was obtained from all patients for whom identifying information is included in this article. Ethical approval for the human sample component of this study was obtained from the Ethics Committee of Stomatology Hospital, Zhejiang University School of Medicine, China (No. 2021-11). The animal experiments were consented to by the Animal Care and Use Committee of Zhejiang University with number ZJU20230115.

References

Al-Dajani M, 2016. Recent trends in sinus lift surgery and their clinical implications. *Clin Implant Dent Relat Res*, 18(1):204-212. https://doi.org/10.1111/cid.12275

Ankrum JA, Ong JF, Karp JM, 2014. Mesenchymal stem cells: Immune evasive, not immune privileged. *Nat Biotechnol*, 32(3):252-260. https://doi.org/10.1038/nbt.2816

Asai S, Shimizu Y, Ooya K, 2002. Maxillary sinus augmentation model in rabbits: Effect of occluded nasal ostium on new bone formation. *Clin Oral Implants Res*, 13(4):405-409. https://doi.org/10.1034/j.1600-0501.2002.130409.x

Chen JM, Huang QY, Zhao YX, et al., 2021. The latest developments in immunomodulation of mesenchymal stem cells in the treatment of intrauterine adhesions, both allogeneic and autologous. *Front Immunol*, 12:785717. https://doi.org/10.3389/fimmu.2021.785717

Chen PH, Tsai WB, 2025. Development of a photocrosslinkable collagen-bone matrix hydrogel for bone tissue engineering. *Polymers (Basel)*, 17(7) https://doi.org/10.3390/polym17070935

Deng Q, Li P, Che M, et al., 2019. Activation of hedgehog signaling in mesenchymal stem cells induces cartilage and bone tumor formation via wnt/beta-catenin. *Elife*, 8 https://doi.org/10.7554/eLife.50208

Derjac-Arama AI, Sarafoleanu C, Manea CM, et al., 2015. Regenerative potential of human schneiderian membrane: Progenitor cells and epithelial-mesenchymal transition. *Anat Rec (Hoboken)*, 298(12):2132-2140. https://doi.org/10.1002/ar.23276

Di Pietro L, Barba M, Prampolini C, et al., 2020. Gli1 and axin2 are distinctive markers of human calvarial mesenchymal stromal cells in nonsyndromic craniosynostosis. *Int J Mol Sci*, 21(12) https://doi.org/10.3390/ijms21124356

Dragonas P, Katsaros T, Schiavo J, et al., 2020. Osteogenic capacity of the sinus membrane following maxillary sinus augmentation procedures: A systematic review. *Int J Oral Implantol (Berl)*, 13(3):213-232.

Falah M, Sohn DS, Srouji S, 2016. Graftless sinus augmentation with simultaneous dental implant placement: Clinical results and biological perspectives. *Int J Oral Maxillofac Surg*, 45(9):1147-1153. https://doi.org/10.1016/j.ijom.2016.05.006

Friedenstein AJ, Chailakhjan RK, Lalykina KS, 1970. The development of fibroblast colonies in monolayer cultures of guinea-pig bone marrow and spleen cells. *Cell Tissue Kinet*, 3(4):393-403. https://doi.org/10.1111/j.1365-2184.1970.tb00347.x

Fujii S, Takebe H, Mizoguchi T, et al., 2023. Bone formation ability of gli1(+) cells in the periodontal ligament after tooth extraction. *Bone*, 173:116786. https://doi.org/10.1016/j.bone.2023.116786

Granchi D, Devescovi V, Baglio SR, et al., 2010. Biological basis for the use of autologous bone marrow stromal cells in the treatment of congenital pseudarthrosis of the tibia. *Bone*, 46(3):780-788.

https://doi.org/10.1016/j.bone.2009.10.044
Guo J, Weng J, Rong Q, et al., 2015. Investigation of multipotent postnatal stem cells from human maxillary sinus membrane. *Sci Rep*, 5:11660. https://doi.org/10.1038/srep11660
Guo Y, Wei J, Liu C, et al., 2023. Metformin regulates bone marrow stromal cells to accelerate bone healing in diabetic mice. *Elife*, 12 https://doi.org/10.7554/eLife.88310
Hameed S, Bakhshalian N, Alwazan E, et al., 2019. Maxillary sinus floor and alveolar crest alterations following extraction of single maxillary molars: A retrospective cbct analysis. *Int J Periodontics Restorative Dent*, 39(4):545-551. https://doi.org/10.11607/prd.3865
Jungner M, Cricchio G, Salata LA, et al., 2015. On the early mechanisms of bone formation after maxillary sinus membrane elevation: An experimental histological and immunohistochemical study. *Clin Implant Dent Relat Res*, 17(6):1092-1102. https://doi.org/10.1111/cid.12218
Lee E, Epanomeritakis IE, Lu V, Khan W, 2023. Bone marrow-derived mesenchymal stem cell implants for the treatment of focal chondral defects of the knee in animal models: A systematic review and meta-analysis. *Int J Mol Sci*, 24(4) https://doi.org/10.3390/ijms24043227
Lee JY, Kim S, Shin SY, et al., 2022. Effectiveness of hydraulic pressure-assisted sinus augmentation in a rabbit sinus model: A preclinical study. *Clin Oral Investig*, 26(2):1581-1591. https://doi.org/10.1007/s00784-021-04131-z
Lemos DR, Eisner C, Hopkins CI, Rossi FMV, 2015. Skeletal muscle-resident mscs and bone formation. *Bone*, 80:19-23. https://doi.org/10.1016/j.bone.2015.06.013
Leocadio ACS, Silva M, Jr., De Oliveira G, Marcantonio E, Jr., 2021. Osseointegration of different implant surfaces in areas grafted with deproteinized bovine bone associated or not with fresh bone marrow-preclinical study in rabbits. *Clin Oral Implants Res*, 32(6):767-775. https://doi.org/10.1111/clr.13746
Lim ST, Kusano K, Taniyama T, et al., 2022. Contribution to bone formation of the schneiderian membrane after sinus augmentation: A histological study in rabbits. *Materials (Basel)*, 15(22) https://doi.org/10.3390/ma15228077
Liu J, Kang J, Zou T, et al., 2025. Functional cobalt-doped hydrogel scaffold enhances concurrent vascularization and neurogenesis. *J Nanobiotechnology*, 23(1):179. https://doi.org/10.1186/s12951-025-03218-z
Liu Y, Wang H, Dou H, et al., 2020. Bone regeneration capacities of alveolar bone mesenchymal stem cells sheet in rabbit calvarial bone defect. *J Tissue Eng*, 11:2041731420930379. https://doi.org/10.1177/2041731420930379
Lv H, Xu J, Wang Y, et al., 2024. Isolation, identification and osteogenic capability analysis of mesenchymal stem cells derived from different layers of human maxillary sinus membrane. *J Clin Periodontol*, 51(6):754-765. https://doi.org/10.1111/jcpe.13956
Makary C, Rebaudi A, Menhall A, Naaman N, 2016. Changes in sinus membrane thickness after lateral sinus floor elevation: A radiographic study. *Int J Oral Maxillofac Implants*, 31(2):331-337. https://doi.org/10.11607/jomi.4108
Maruyama T, Jiang M, Abbott A, et al., 2017. Rap1b is an effector of axin2 regulating crosstalk of signaling pathways during skeletal development. *J Bone Miner Res*, 32(9):1816-1828. https://doi.org/10.1002/jbmr.3171
Maurer T, Stoffel MH, Belyaev Y, et al., 2018. Structural characterization of four different naturally occurring porcine collagen membranes suitable for medical applications. *PLoS One*, 13(10):e0205027. https://doi.org/10.1371/journal.pone.0205027
Moon YS, Sohn DS, Moon JW, et al., 2014. Comparative histomorphometric analysis of maxillary sinus augmentation with absorbable collagen membrane and osteoinductive replaceable bony window in rabbits. *Implant Dent*, 23(1):29-36. https://doi.org/10.1097/ID.0000000000000031
Palma VC, Magro-Filho O, De Oliveria JA, et al., 2006. Bone reformation and implant integration following maxillary sinus membrane elevation: An experimental study in primates. *Clin Implant Dent Relat Res*, 8(1):11-24. https://doi.org/10.2310/j.6480.2005.00026.x
Pereira RDS, De Carvalho M, Hochuli-Vieira E, et al., 2024. Histomorphometric and micro-ct evaluation of cerabone and bio-oss in maxillary sinus lifting: A randomized clinical trial. *Medicina (Kaunas)*, 60(11) https://doi.org/10.3390/medicina60111834
Qian SJ, Mo JJ, Shi JY, et al., 2018. Endo-sinus bone formation after transalveolar sinus floor elevation without grafting with simultaneous implant placement: Histological and histomorphometric assessment in a dog model. *J Clin Periodontol*, 45(9):1118-1127. https://doi.org/10.1111/jcpe.12975
Reinders ME, De Fijter JW, Roelofs H, et al., 2013. Autologous bone marrow-derived mesenchymal stromal cells for the treatment of allograft rejection after renal transplantation: Results of a phase i study. *Stem Cells Transl Med*, 2(2):107-111. https://doi.org/10.5966/sctm.2012-0114

Rong Q, Li X, Chen SL, et al., 2015. Effect of the schneiderian membrane on the formation of bone after lifting the floor of the maxillary sinus: An experimental study in dogs. *Br J Oral Maxillofac Surg*, 53(7):607-612. https://doi.org/10.1016/j.bjoms.2015.02.010

Saha S, Yang XB, Wijayathunga N, et al., 2019. A biomimetic self-assembling peptide promotes bone regeneration in vivo: A rat cranial defect study. *Bone*, 127:602-611. https://doi.org/10.1016/j.bone.2019.06.020

Sakuma S, Ferri M, Imai H, et al., 2020. Involvement of the maxillary sinus ostium (mso) in the edematous processes after sinus floor augmentation: A cone-beam computed tomographic study. *Int J Implant Dent*, 6(1):35. https://doi.org/10.1186/s40729-020-00233-7

Scala A, Botticelli D, Rangel IG, Jr., et al., 2010. Early healing after elevation of the maxillary sinus floor applying a lateral access: A histological study in monkeys. *Clin Oral Implants Res*, 21(12):1320-1326. https://doi.org/10.1111/j.1600-0501.2010.01964.x

Scala A, Botticelli D, Faeda RS, et al., 2012. Lack of influence of the schneiderian membrane in forming new bone apical to implants simultaneously installed with sinus floor elevation: An experimental study in monkeys. *Clin Oral Implants Res*, 23(2):175-181. https://doi.org/10.1111/j.1600-0501.2011.02227.x

Srouji S, Kizhner T, Ben David D, et al., 2009. The schneiderian membrane contains osteoprogenitor cells: In vivo and in vitro study. *Calcif Tissue Int*, 84(2):138-145. https://doi.org/10.1007/s00223-008-9202-x

Srouji S, Ben-David D, Lotan R, et al., 2010. The innate osteogenic potential of the maxillary sinus (schneiderian) membrane: An ectopic tissue transplant model simulating sinus lifting. *Int J Oral Maxillofac Surg*, 39(8):793-801. https://doi.org/10.1016/j.ijom.2010.03.009

Suchanecka M, Grzelak J, Farzaneh M, et al., 2025. Adipose derived stem cells - sources, differentiation capacity and a new target for reconstructive and regenerative medicine. *Biomed Pharmacother*, 186:118036. https://doi.org/10.1016/j.biopha.2025.118036

Sui BD, Hu CH, Liu AQ, et al., 2019. Stem cell-based bone regeneration in diseased microenvironments: Challenges and solutions. *Biomaterials*, 196:18-30. https://doi.org/10.1016/j.biomaterials.2017.10.046

Summers RB, 1994. A new concept in maxillary implant surgery: The osteotome technique. *Compendium*, 15(2):152, 154-156, 158 passim; quiz 162.

Tatum H, Jr., 1986. Maxillary and sinus implant reconstructions. *Dent Clin North Am*, 30(2):207-229.

Tooze RS, Miller KA, Swagemakers SMA, et al., 2023. Pathogenic variants in the paired-related homeobox 1 gene (prrx1) cause craniosynostosis with incomplete penetrance. *Genet Med*, 25(9):100883. https://doi.org/10.1016/j.gim.2023.100883

Wang J, Sun Y, Liu Y, et al., 2022. Effects of platelet-rich fibrin on osteogenic differentiation of schneiderian membrane derived mesenchymal stem cells and bone formation in maxillary sinus. *Cell Commun Signal*, 20(1):88. https://doi.org/10.1186/s12964-022-00844-0

Weng Y, Wang H, Wu D, et al., 2022. A novel lineage of osteoprogenitor cells with dual epithelial and mesenchymal properties govern maxillofacial bone homeostasis and regeneration after msfl. *Cell Res*, 32(9):814-830. https://doi.org/10.1038/s41422-022-00687-x

Xie C, Liang R, Ye J, et al., 2022. High-efficient engineering of osteo-callus organoids for rapid bone regeneration within one month. *Biomaterials*, 288:121741. https://doi.org/10.1016/j.biomaterials.2022.121741

Yang C, Li Z, Liu Y, et al., 2022. Single-cell spatiotemporal analysis reveals cell fates and functions of transplanted mesenchymal stromal cells during bone repair. *Stem Cell Reports*, 17(10):2318-2333. https://doi.org/10.1016/j.stemcr.2022.08.008

Yin L, Zhou ZX, Shen M, et al., 2019. The human amniotic mesenchymal stem cells (hamscs) improve the implant osseointegration and bone regeneration in maxillary sinus floor elevation in rabbits. *Stem Cells Int*, 2019:9845497. https://doi.org/10.1155/2019/9845497

Yu M, Ma L, Yuan Y, et al., 2021. Cranial suture regeneration mitigates skull and neurocognitive defects in craniosynostosis. *Cell*, 184(1):243-256 e218. https://doi.org/10.1016/j.cell.2020.11.037

Yuan Y, Loh YE, Han X, et al., 2020. Spatiotemporal cellular movement and fate decisions during first pharyngeal arch morphogenesis. *Sci Adv*, 6(51) https://doi.org/10.1126/sciadv.abb0119

Zhao H, Feng J, Ho TV, et al., 2015. The suture provides a niche for mesenchymal stem cells of craniofacial bones. *Nat Cell Biol*, 17(4):386-396. https://doi.org/10.1038/ncb3139

Zhu J, Xiong J, Ji W, 2023. A systematic review of bone marrow stromal cells and periosteum-derived cells for bone regeneration. *Tissue Eng Part B Rev*, 29(2):103-122. https://doi.org/10.1089/ten.TEB.2022.0115

Supplementary information

Figs. S1 and S2